Sustainable Carbon Materials

Original Research

Open Access

https://doi.org/10.48130/scm-0025-0003

Sustainable carbon materials for magnetic adsorbent-based pentachlorophenol removal from wastewater

Tunnisha Dasgupta[1], Himadri Rajput[1], Pubudi Perera[1], Xiaohong Sun[2] and Quan (Sophia) He[1*]

Received: 13 June 2025

Revised: 26 July 2025

Accepted: 20 September 2025

Published online: 27 October 2025

Abstract

The growing water scarcity caused by human activities and urbanization has made it essential to develop sustainable and cost-effective strategies for wastewater treatment and reuse. This study involved converting biomass waste from agricultural and forestry sources into magnetic carbon-based adsorbents through hydrothermal carbonization (HTC). During the HTC process, iron was incorporated to impart magnetic properties to the resulting hydrochar, enabling post-treatment recovery using an external magnet. Hydrochars derived from flax shives (FS-Fe-HC), and eucalyptus (ES-Fe-HC) were tested for their efficiency in adsorbing pentachlorophenol (PCP) from wastewater. The structural, morphological, and chemical characteristics of the prepared hydrochar were characterized through scanning electron microscopy-electron diffraction spectroscopy (SEM-EDS), Fourier transform infrared spectroscopy (FTIR), X-ray diffraction (XRD), X-ray photoelectron spectroscopy (XPS), Brunauer-Emmett-Teller (BET), and vibrating sample magnetometry (VSM) techniques. Batch adsorption experiments revealed maximum PCP removal efficiencies of 95% for FS-Fe-HC, and 88.5% for ES-Fe-HC under optimized conditions. The adsorption performance was found to be influenced by surface functional groups, active adsorption sites, and pH-dependent surface charge. Both hydrochars exhibited excellent reusability over six consecutive adsorption-desorption cycles, with negligible iron leaching, confirming their stability and practical applicability. This study demonstrates the potential of HTC as a sustainable approach for valorizing lignocellulosic waste into effective bio-adsorbents for wastewater remediation, addressing both environmental and industrial challenges. The novelty lies in utilizing dual biomass waste, magnetic recovery capability, and high reusability with minimal iron leaching, thereby contributing to circular economy practices in water treatment.

Keywords: Adsorption, Pentachlorophenol, Flax shives, Eucalyptus, Magnetic hydrochar

Highlights

- Efficient PCP removal using flax shives and eucalyptus-derived hydrochars.
- Well-developed mesoporous structures were observed.
- Easy recovery of magnetic hydrochar using an external magnet after treatment.
- No iron leaching from hydrochar was observed.

* Correspondence: Quan (Sophia) He (quan.he@dal.ca)

Full list of author information is available at the end of the article.

Graphical abstract

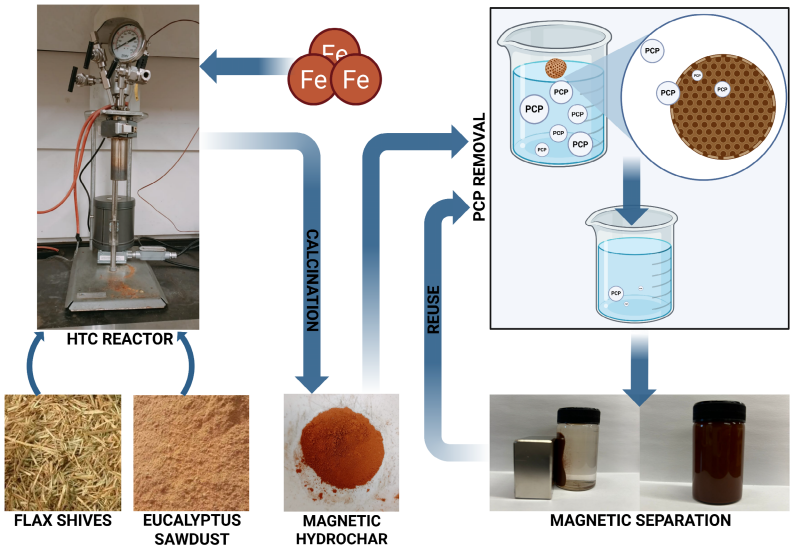

Introduction

In this era of rapid industrialization and urbanization, the population has experienced an unprecedented increase, resulting in a corresponding rise in water demand[1]. Industrial activities contribute to about 20% of freshwater being withdrawn, which is either treated and reused, or disposed of in a sustainable manner. However, without proper management, wastewater containing several synthetic chemical contaminants could make their way into natural water bodies[2]. Pentachlorophenol (PCP) is one of many contaminants that have infiltrated the water bodies and soils through industrial discharge, agricultural activities, and other improper disposal practices[3]. Its presence has been detected in rainwater, surface water, drinking water, sediments, soil, and food, posing a risk of causing detrimental impacts on the environment[4]. Therefore, identifying effective strategies for its removal is imperative. Several methods have been explored to facilitate PCP remediation, such as electrocatalytic treatment[5], combined anaerobic-aerobic treatment[4], phytoremediation[6], bioaugmentation[7], and adsorption. Adsorption is one of the oldest and most widely employed methods due to its numerous benefits, including lower operational costs, sustainability, and fewer secondary pollutant productions[8]. Among the various adsorbents, activated carbon is considered the industry standard, as it can be easily modified to enhance the adsorption capacity; however, it is difficult to separate after use, and is not a cost-effective option[9]. Therefore, the application of biosorbents derived from biomass waste has gained significant attention due to their cost-effectiveness and sustainability[10]. The use of biosorbents not only addresses the immediate challenge but also promotes a circular economic approach by reducing the burden on landfills and preserving natural ecosystems[11].

Hydrothermal carbonization (HTC) is a thermochemical process that converts waste biomass into hydrochar (HC), which can be engineered with desirable surface and structural properties for use as a biosorbent. The characteristics of hydrochar, such as surface area, porosity, and functional groups, can be tuned by selecting appropriate biomass feedstocks, and controlling HTC conditions. Flax shives and eucalyptus sawdust, due to their abundance in nature and favorable physicochemical properties, have been extensively explored by the scientific community. Sourced from the agricultural and forestry sectors, these biomass wastes have various benefits when valorized for wastewater treatment[12]. The pore structure and lignin content of flax shives are highly favorable for the adsorption of heavy metals, dyes, and other pollutants[13]. Similarly, the hydrochar derived from eucalyptus is advantageous due to its stability and high surface area, which enables efficient adsorption of organic contaminants and heavy metals[14]. Modified hydrochar, especially those doped with metal oxides such as iron, has a higher surface area, additional reactive functional groups, enhanced porosity, easy regenerative properties, and reusability. More importantly, it also possesses magnetic properties for easy separation[15,16]. Several studies have investigated hydrochars derived from flax shives and eucalyptus sawdust due to their availability and carbon-rich composition[17,18]. These studies mainly examined non-magnetic hydrochar for the removal of pollutants such as dyes and heavy metals. However, the synthesis of magnetic hydrochar from these biomass materials remains unexplored, particularly those doped with iron, which can impart magnetic properties for easy separation, and enhance adsorption through redox-active surface functionalities.

In this study, iron-based biosorbents were synthesized from flax shives, and eucalyptus sawdust through HTC. Ferrous sulphate heptahydrate ($Fe_2SO_4 \cdot 7H_2O$) and anhydrous ferric chloride ($FeCl_3$) were incorporated to introduce magnetic properties to the hydrochar. The main objectives of this investigation were: 1) to synthesize magnetic hydrochars derived from flax shives and eucalyptus sawdust via hydrothermal processes; 2) to characterize the physicochemical properties of the resulting hydrochars; and 3) to evaluate their efficacy in removing PCP from wastewater and their reusability potential.

Materials and methods

Chemicals

Ferrous sulphate heptahydrate ($Fe_2SO_4 \cdot 7H_2O$, ≥ 99%) and anhydrous ferric chloride ($FeCl_3$, 98%) were purchased from Acros Organics and

Thermo Scientific, respectively. NaOH pellets were acquired from Anachemia. Acetone (≥ 99.5%) and PCP (97%) were obtained from Sigma-Aldrich. All the reagents used are of analytical grade and were used as provided, without any further modifications. Flax shives were collected from TapRoot Farms, Nova Scotia, Canada, and eucalyptus sawdust was provided by the Laboratory of Solid Residues and Composites at São Paulo State University, Brazil. The obtained flax shives and eucalyptus sawdust were ground and sieved in a 125 mm mesh. The findings of proximate and biochemical analysis[19–22] of the raw materials are presented in Table 1.

Table 1 Proximate and biochemical analysis of flax shives and eucalyptus sawdust

Biomass	Flax shives	Eucalyptus sawdust
Proximate analysis (wt%)		
Moisture	1.04 ± 0.15	1.36 ± 0.04
Volatile	95.99	97.64
Fixed carbon	2.48	1.91
Ash	1.78 ± 0.25	0.72 ± 0.27
Biochemical analysis (wt%)		
Cellulose	45 ± 5.92	42 ± 5.38
Hemicellulose	29.67 ± 4.91	27 ± 5.01
Lignin	25 ± 1.82	31 ± 2.45

Hydrochar synthesis

Magnetic hydrochar was synthesized using two representatives for agricultural and forestry: flax shives and eucalyptus sawdust (Fig. 1). The ground and sieved biomass was mixed with distilled water (1:8). Following this, Fe_2SO_4•$7H_2O$ (9.95 g/L), and anhydrous $FeCl_3$ (19.49 g/L) were added to the mixture. After dispersing the iron salts, 0.072 mL of 1 M NaOH was introduced while the mixture was stirred using an electromagnetic stirrer for 30 min. The resulting suspension was transferred to an HTC reactor, where it was thermally treated at 200 °C for 24 h in a nitrogen-purged inert atmosphere[23]. After cooling, the obtained hydrochar was washed with distilled water and soaked in acetone for 12 h. It was then filtered, rinsed with deionized water, and dried in an oven at 105 °C for 6 h. The dried hydrochar was subsequently calcined in a muffle furnace at 400 °C for 1 h, with a heating rate of 5 °C/min. The final products were labelled FS-Fe-HC and ES-Fe-HC.

Characterization of synthesis FS-Fe-HC and ES-Fe-HC

Several processes were employed for determining the physical and chemical characteristics of hydrochar. Fourier transform infrared spectroscopy (FTIR, PerkinElmer Spectrum 10.5.2) was used to study the functional groups present on the surface of hydrochar before and after iron doping over a wavelength range of 400–4,000 cm^{-1}. The crystal structure of the synthesized hydrochar was examined by X-ray diffraction (XRD, Siemens D500, Germany) under Cu-K_α radiation at a 2θ range of 5–80°. The surface morphology and structure were analyzed by scanning electron microscopy (SEM, Oxford Instruments). The elemental distribution was studied by electron diffraction spectroscopy (EDS). To study the bonds formed on the surface of the hydrochar and their binding energies, X-ray photoelectron spectroscopy (XPS, MultiLab ESCA 2000, UK) was employed. The magnetic properties of the hydrochar were studied by a vibrating sample magnetometer (VSM, Lakeshore, 8600). The specific surface area, pore diameter, and volume were analyzed using a Microtrac MRB BELSORP-Mini X Brunauer-Emmett-Teller (BET) analyzer. Inductively coupled plasma optical emission spectroscopy (ICP-OES, Agilent 5110) was used to study whether any iron introduced during synthesis was leached during or after treatment.

Batch experiments

Experiments were performed to investigate how reaction conditions affect the removal of PCP using FS-Fe-HC and ES-Fe-HC. The adsorbent dose was varied from 0.2 to 0.8 g/L for FS-Fe-HC and from 0.1 to 0.5 g/L for ES-Fe-HC. The effect of pH was studied in the range of 4 to 10, while the initial PCP concentration varied from 4 to 14 mg/L for both hydrochars. The effect of contact time was studied at various time intervals, ranging from 5 to 1,680 min. The collected samples were filtered through a 0.45 μm pore size filter, and the concentration of PCP was measured by using a UV-Vis spectrophotometer at 214 nm. A study was conducted to evaluate the recyclability of both FS-Fe-HC and ES-Fe-HC, involving five adsorption cycles where the same hydrochar was used for PCP removal and subsequently regenerated in 5% methanol. The point of zero charge (pH_{PZC}) was determined using the method as described in our previous study[24]. The percentage removal (R, %) of PCP was determined by using the following Eq. (1):

$$R(\%) = \frac{C_0 - C_e}{C_0} \times 100 \quad (1)$$

where, C_0 is the initial PCP concentration in mg/L, and C_e is the equilibrium PCP concentration in mg/L.

The data collected from adsorption experiments were fitted to the non-linear pseudo-first-order and pseudo-second-order models.

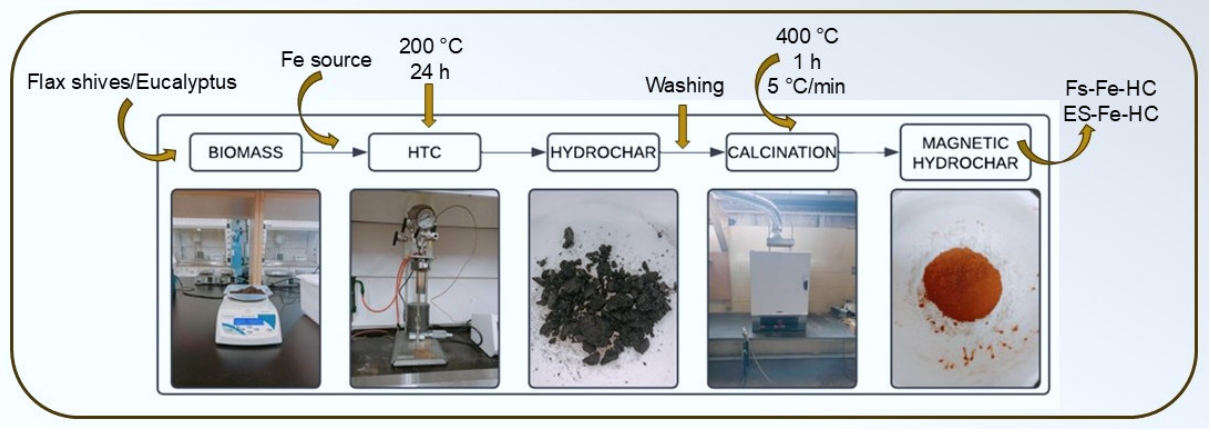

Fig. 1 Synthesis of magnetic hydrochar through hydrothermal carbonization.

Non-linearized forms of Langmuir, Freundlich, and Temkin isotherm models were applied to the PCP adsorption data, as described in our recent study[25].

Results and discussion

Characterization of FS-Fe-HC and ES-Fe-HC

FTIR was employed to identify the surface functional groups present in the hydrochar samples. For the FS-HC sample, prominent absorption peaks were detected at 1035.29, 607.66, 553.49, and 472.23 cm^{-1}. These peaks correspond to aliphatic C–O stretching, Fe_3O_4, Fe–O vibration, and Si–O–Si bonds, respectively (Fig. 2a)[25–27]. After iron doping, FS-Fe-HC samples displayed additional peaks at 3,397.54, 2,335.43, 1,637.76, and 1,044.32 cm^{-1}, which are attributed to –OH stretching, C=O stretching (from ketones and aromatics), and –COOH functional groups[28]. Notably, Fe–O and Si–O–Si vibrations were still evident at 548.56 and 472.23 cm^{-1}, indicating that partial original functionalities were retained after doping[26].

Similarly, the FTIR spectrum of ES-HC (Eucalyptus Sawdust Hydrochar) showed –OH stretching vibration at 3,442.68 cm^{-1}, along with several peaks that correspond to various surface functional groups (Fig. 2a)[28]. Peaks at 2,978.93, 2,218.88 cm^{-1}, and within the range of 1,793.09–1,696.96 cm^{-1} represent the aliphatic $–CH_2$ stretches, C–N bonds, and carbonyl (C=O) groups, respectively[23,28]. Additional peaks at 1,596.96–1,411.82, 1,255.27, 1,030.37, and 594.22–503.30 cm^{-1} indicate the presence of aromatic C=C stretching (lignin-related), ether linkages (C–O–C), carboxylic acid groups (–COOH), and Si–O–Si bending vibrations[28]. A final band in the range of 453.70–435.14 cm^{-1} was assigned to alkyl halide groups. After iron doping, the ES-Fe-HC spectrum showed that the retained functional groups were similar to those of FS-Fe-HC, including –OH stretching (3,447.60 cm^{-1}), C–N bonds (2,362.52 and 2,340.36 cm^{-1}), Si–O–Si bending (526.40 cm^{-1}), and alkyl halides (436.11 cm^{-1})[25,29]. Importantly, no new significant peaks were observed following iron doping, indicating that the major structural features remained largely unchanged.

XRD analysis was conducted to investigate the crystalline phases present in FS-Fe-HC and ES-Fe-HC, with the findings presented in Fig. 2b. In FS-Fe-HC, the diffraction peaks at 25.49, 26.63, and 27.43° (2θ) correspond to graphitized or amorphous graphite-like carbon structures, which may also include contributions from residual cellulose[30]. Peaks at 30.31, 33.11, 35.56°, and within the range of 52.36–59.89° indicate the presence of crystalline Fe_2O_3 phases, while a peak at 63.03° confirms the presence of zero-valent iron (Fe^0)[31]. In ES-Fe-HC, the peaks at 24.01 and 27.43° suggest disordered graphitic carbon with some cellulose-derived structures[30]. The peaks at 30.14, 33.03, and 35.56° are again attributed to Fe_2O_3, while those at 40.82 and 49.48° correspond to turbostratic carbon—a characteristic form of disordered graphite in hydrothermal carbons. Further peaks for Fe_2O_3 appear at 54.11, 57.53, and 62.60°, and a peak at 64.08° indicates the formation of Fe^0, suggesting partial reduction during HTC[31,32]. Overall, these patterns confirm the coexistence of iron oxide and disordered carbon phases. After one adsorption cycle, the XRD patterns of FS-Fe-HC-Reused and ES-Fe-HC-Reused remained largely unchanged. The key peaks for Fe_2O_3, graphitic/turbostratic carbon, and Fe^0 were retained, showing only minor variations in intensity. This structural stability highlights the reusability of the hydrochar without significant crystalline degradation.

The XPS survey spectra (Fig. 2c) of the hydrochar revealed the presence of four main elements: carbon (C 1s), oxygen (O 1s), nitrogen (N 1s), and iron (Fe 2p), with binding energy features indicative of their chemical states. All samples exhibited a dominant C 1s (Fig. 3a) peak at 284.8 eV, which corresponds to non-oxygenated carbon atoms, such as C–C and C=C bonds[33]. Peaks at 286.3 and 287.7 eV were attributed to C–O–C (ether) and C=O (carbonyl) groups, respectively, while the peak at 289.0 eV was assigned to O–C=O (carboxyl) functionalities. The presence of these oxygenated groups suggests that partial oxidation of biomass occurred during the HTC process[33]. In FS-HC and ES-HC, the O 1s spectra (Fig. 3b) displayed peaks at approximately 531.4 and 533.2–534.5 eV, which were attributed to lattice oxygen and surface-adsorbed oxygen, respectively[34]. After iron doping, FS-Fe-HC and ES-Fe-HC exhibited O 1s peaks at 530.0–530.7 eV (adsorbed oxygen) and 531.7–532.1 eV (lattice oxygen), indicating interactions between oxygen and iron oxide surfaces. The slight shift towards lower binding energies indicates enhanced metal–oxygen interactions due to iron incorporation[24]. The N 1s spectra (Fig. 3c) of ES-HC displayed peaks at 398.6 and 400.7 eV, corresponding to pyridinic and pyrrolic nitrogen species, respectively. In contrast, the FS-HC showed peaks at 399.9 and 401.5 eV, aligned with pyrrolic and graphitic nitrogen configurations[35]. Although these nitrogen functionalities are present in low concentrations, they may contribute to the adsorption properties and reactivity of the hydrochar. The Fe 2p spectra (Fig. 3d) of FS-Fe-HC and ES-Fe-HC showed characteristic peaks at 712.32 eV (Fe $2p_{3/2}$) and 725.85 eV (Fe $2p_{1/2}$), confirming the presence of iron species. Deconvolution identified Fe^{2+} at 710.3 and 723.49 eV and Fe^{3+} at 718.3 and 726.13 eV, which indicates the formation of mixed-valence iron oxides, such as magnetite (Fe_3O_4), during the hydrothermal process. This coexistence of valence states

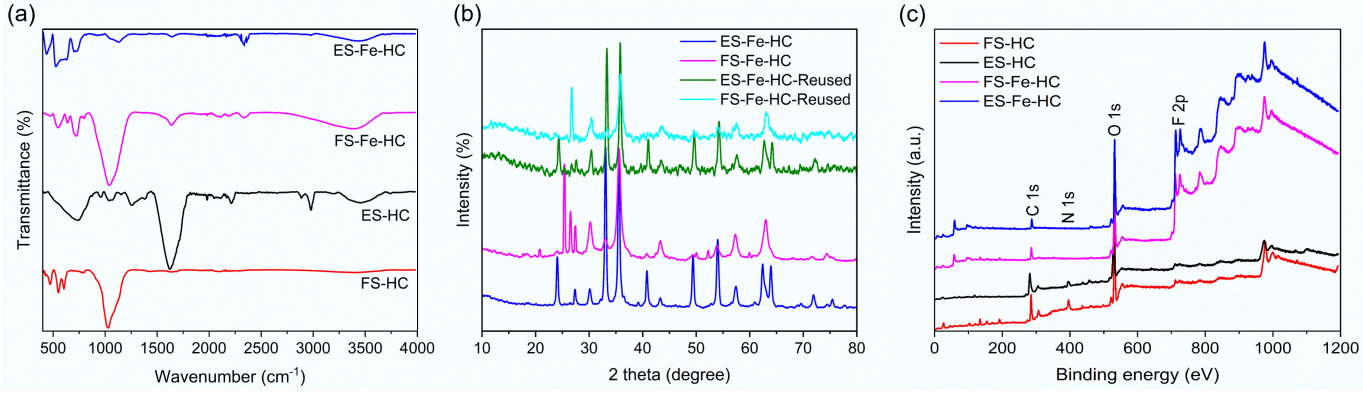

Fig. 2 (**a**) FTIR, (**b**) XRD, and (**c**) XPS analysis of flax shives and eucalyptus sawdust hydrochar.

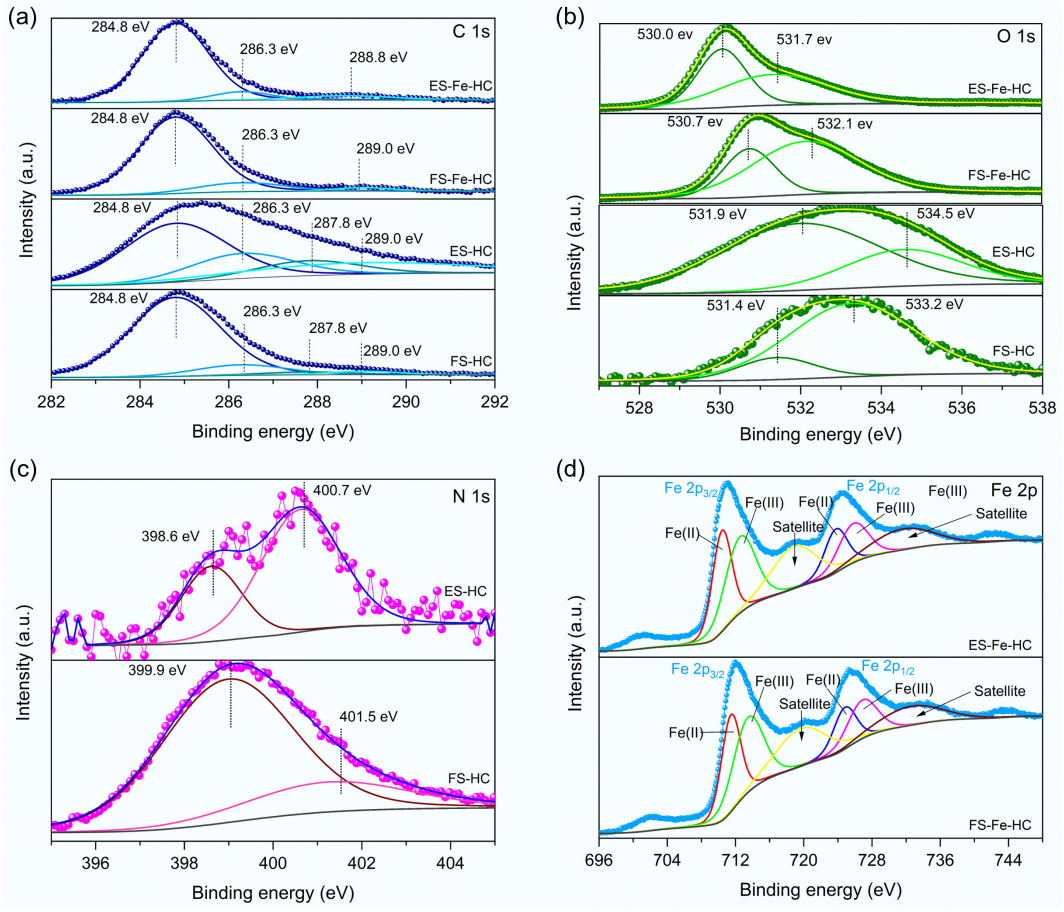

Fig. 3 The high-resolution XPS spectra of (**a**) C 1s, (**b**) O 1s, (**c**) N 1s, and (**d**) Fe 2p.

is consistent with the enhanced redox behaviour observed in iron-doped carbonaceous materials[36].

The VSM analysis was employed to analyze the magnetic properties of the synthesized hydrochar. Saturation magnetization (M_S) refers to the state where FS-Fe-HC and ES-Fe-HC may attain their maximum magnetization as the external magnetic field increases[37]. M_S can serve as a surrogate indicator for predicting the separability of hydrochar from the liquid phase using permanent magnetic bars[38]. For FS-Fe-HC (Fig. 4a), the calculated values of M_S, coercivity (H_C), and remanence (M_r) were 0.123 emu/g, 14.36 Oe, and 0.006 emu/g, respectively. For ES-Fe-HC (Fig. 4b), the calculated values of M_S, H_C, and M_r were 0.2555 emu/g, 65.43 Oe, and 0.038 emu/g, respectively. The low remanence values of both hydrochars indicate that FS-Fe-HC and ES-Fe-HC retain low residual magnetism when the external magnetic field is eliminated[39]. Despite the low M_S values, both hydrochars were rapidly separated from the bulk liquid within a few seconds after the adsorption reaction when an external magnet was applied.

The textural properties of the hydrochar were evaluated using BET analysis, with the results summarized in Table 2. A significant increase in surface area and pore structure was noted following iron modification of the hydrochar.

The surface area of ES-HC and FS-HC was found to be extremely low, measuring 0.8796 and 4.3803 m^2/g, respectively, with corresponding total pore volumes of 0.0548 and 0.0269 cm^3/g. Their large average pore diameters of 125.52 and 12.29 nm indicate a dominance of macroporous and mesoporous structures. This observation aligns with existing literature on hydrochar derived from lignocellulosic biomass that underwent limited activation during hydrothermal carbonization[40,41]. After calcination, there was a significant enhancement in surface characteristics. FS-Fe-HC exhibited the highest BET surface area of 118.49 m^2/g, followed by ES-Fe-HC with 87.74 m^2/g. Correspondingly, both hydrochars showed higher pore volumes (0.4271–0.4393 cm^3/g) and reduced average pore diameters (7.21–10.01 nm), which indicates the formation of well-developed mesopores (Fig. 4c, d). This enhancement can be attributed to the catalytic effect of iron salts, which promote pore formation during the carbonization process and prevent structural collapse by stabilizing intermediate carbon structures[42–44]. Such improvements in textural properties are critical for adsorption-based applications, as higher surface area and increased mesoporosity enhance the availability of active sites and facilitate mass transfer in aqueous environments[45].

The surface morphology of the hydrochar before and after iron modification was examined through SEM analysis. Hydrochar derived from flax shives (Fig. 5a–f), and eucalyptus (Fig. 5g–l) showed irregularly shaped rough surfaces with unevenly scattered pores and asymmetrical cavities. This can be attributed to the polymerization of thermally degraded products from lignin, hemicellulose, and cellulose[46]. When iron was introduced, clusters of interconnected spherical microstructures were observed on the surface of the hydrochar. Porous structures between the microspheres indicated an increase in the surface area of hydrochar, which may facilitate the adsorption process[47]. EDS analysis confirmed the presence of 30.46 and 32.8 wt% Fe in FS-Fe-HC and ES-Fe-HC, respectively.

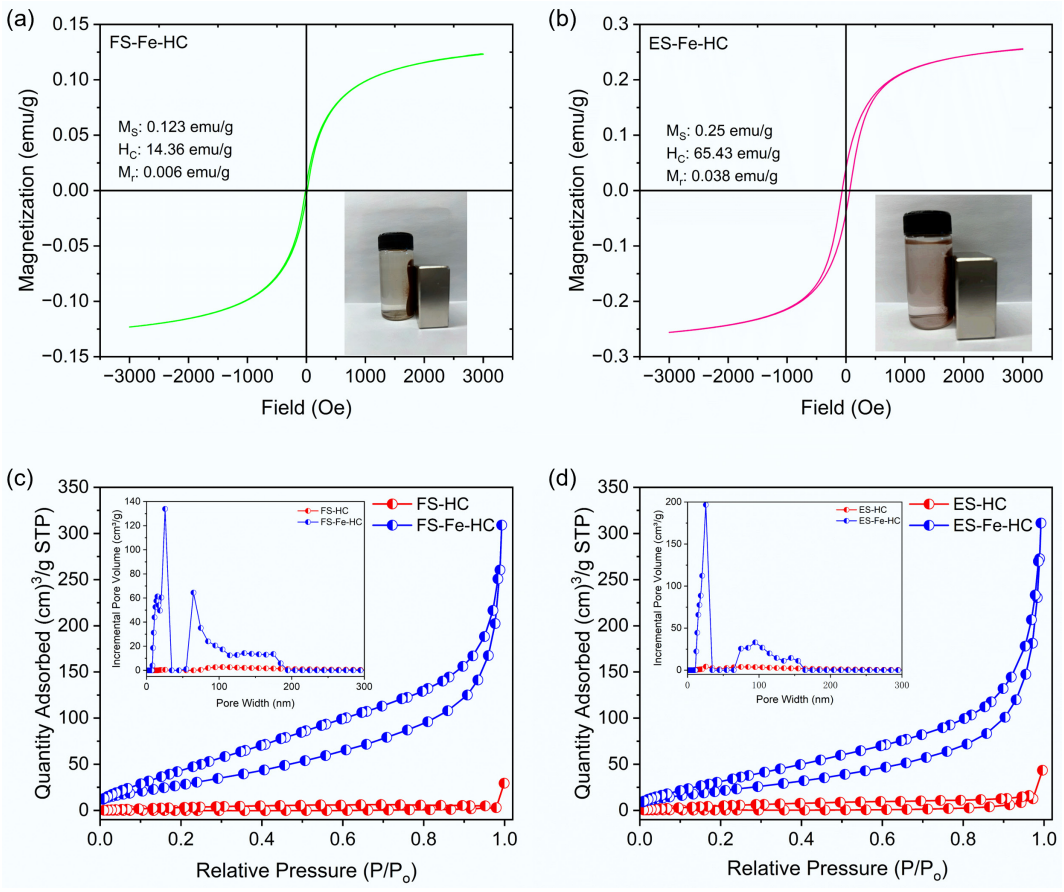

Fig. 4 (**a**), (**b**) VSM, and (**c**), (**d**) BET analysis of flax shives and eucalyptus sawdust hydrochar.

Influence of adsorbent dosage on removal efficiency

The influence of varying adsorbent dosages was investigated for FS-Fe-HC in the range of 0.2 to 0.8 g/L and for ES-Fe-HC from 0.1 to 0.5 g/L (Fig. 6a). Due to an increasing number of functional groups and active sites for adsorption in the reaction solution, an increasing trend in the removal efficiency was observed for both FS-FE-HC and ES-Fe-HC as the dosage increased[48]. However, no additional increase in efficiency was observed beyond 0.4 g/L (FS-Fe-HC) and 0.3 g/L (ES-Fe-HC). This is probably due to the availability of an excessive number of binding sites at higher dosages that cannot be fully occupied at a constant PCP concentration[49]. As a result, dosages of 0.4 and 0.3 g/L were identified as the optimized amounts, leading to 95% and 88% PCP removal within 60 and 35 min at pH 4 for FS-Fe-HC and ES-Fe-HC, respectively. The slightly lower removal efficiency observed for ES-Fe-HC may be due to its comparatively lower surface area and fewer surface oxygen-containing functional groups relative to FS-Fe-HC.

Table 2 BET analysis of FS-HC, ES-HC, FS-Fe-HC, and ES-Fe-HC

Biomass	BET surface area (S_{BET}) (m^2/g)	Total pore volume (cm^3/g)	Average pore diameter (nm)
FS-HC	4.3803	0.0269	12.29
ES-HC	0.8796	0.0548	125.52
FS-Fe-HC	118.49	0.4271	7.21
ES-Fe-HC	87.74	0.4393	10.01

Influence of initial PCP concentration on removal efficiency

For both FS-Fe-HC and ES-Fe-HC, an increasing trend in removal efficiency was observed as the initial PCP concentration increased. For FS-Fe-HC, PCP removal reached 97% while for ES-Fe-HC it reached 92.4%, when the PCP initial concentration was increased from 4 to 12 mg/L (Fig. 6b). This increase is attributed to the elevated PCP concentration, which enhances the diffusion of PCP from the bulk liquid to the adsorbent surface by increasing the driving force of the concentration gradient[50]. A further increase in the PCP concentration beyond 12 mg/L results in a reduction in removal efficiency for both hydrochars, indicating the saturation of the available binding sites. It was concluded that the initial concentration of PCP influences the removal efficiency during the adsorption process.

Influence of pH on removal efficiency

The adsorption of PCP decreases as the pH increases for both FS-Fe-HC and ES-Fe-HC. Specifically, the removal efficiency of PCP dropped from 95% to 26.5% for FS-Fe-HC and from 88.4% to 22.8% for ES-Fe-HC when pH was raised from 4 to 10 (Fig. 6c). The two most common properties inherent to ionizable organic contaminants are solubility and distribution ratios, both of which are significantly affected by the solution's pH. As the pH value increases, the distribution ratio of PCP in water decreases, while its solubility increases, thereby affecting the adsorption[51]. The primary form in which PCP exists in nature is PCP^0 at pH < pK_a and PCP^- at pH > pK_a[52]. Various studies indicate that since PCP is a weak hydrophobic organic acid (pK_a:4.7), which remains

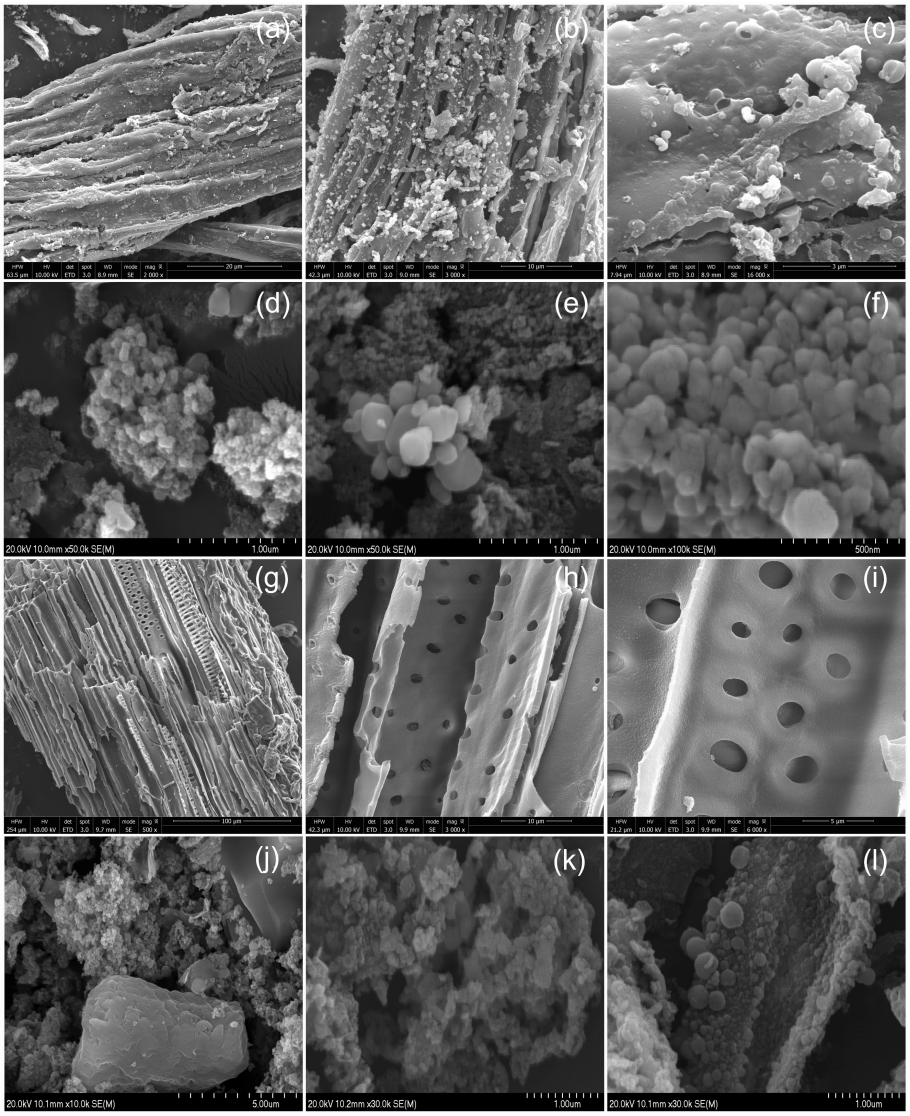

Fig. 5 The surface morphology of (**a**)–(**c**) FS-HC, (**d**)–(**f**) FS-Fe-HC, (**g**)–(**i**) ES-HC, and (**j**)–(**l**) ES-Fe-HC.

mostly neutral in the acidic range of pH, it shows higher rates of adsorption compared to when the pH is basic, where it exists as an anion[24]. This is attributed to the surface charge of the hydrochar becoming more negative as the pH increases, which leads to the repulsion of more pentachlorophenolate anions[53]. The higher solubility and reduced hydrophobicity of the ionized (anionic) form of PCP are responsible for the significant decrease in PCP adsorption on hydrochar as the pH rises[51].

Point of zero charge of FS-Fe-HC and ES-Fe-HC

The point of zero charge was investigated and found to be 4.2 for FS-Fe-HC and 3.9 for ES-Fe-HC, as shown in Fig. 6d. At a pH_{pzc} around 4, both hydrochars have neutral surface charges. And below this pH, they acquire positive charges, which enhance the adsorption of the negatively charged PCP through electrostatic attraction. Therefore, FS-Fe-HC and ES-Fe-HC can effectively capture anionic PCP at a pH level below 4. This finding supports the observation obtained during pH optimization, where the highest removal efficiency was achieved at pH 4.

Influence of contact time

The study examined how contact time affects the removal of PCP using FS-Fe-HC and ES-Fe-HC under optimized conditions. The adsorption process occurred in two phases. A rapid phase lasting 10–15 min, during which more than 80% of PCP was removed, followed by a flat phase that extended up to 210 min (Fig. 6e). The quick uptake of PCP during the rapid phase was observed due to the availability of abundant vacant binding sites[54]. However, as the contact time increased, the remaining binding sites became harder to occupy due to repulsive forces between the PCP in the liquid and those on the adsorbent surface. Eventually, the hydrochar surface reached saturation, leading to the establishment of equilibrium. When the contact time was extended to 1,680 min, 11.6% and 21% desorption was observed in the case of FS-Fe-HC and ES-Fe-HC. This desorption likely occurred due to the release of loosely bound PCP and the saturation of the adsorbent's capacity to further retain adsorbed PCP[55]. Table 3 summarizes the comparative potential of different biomass waste-based adsorbents for PCP removal.

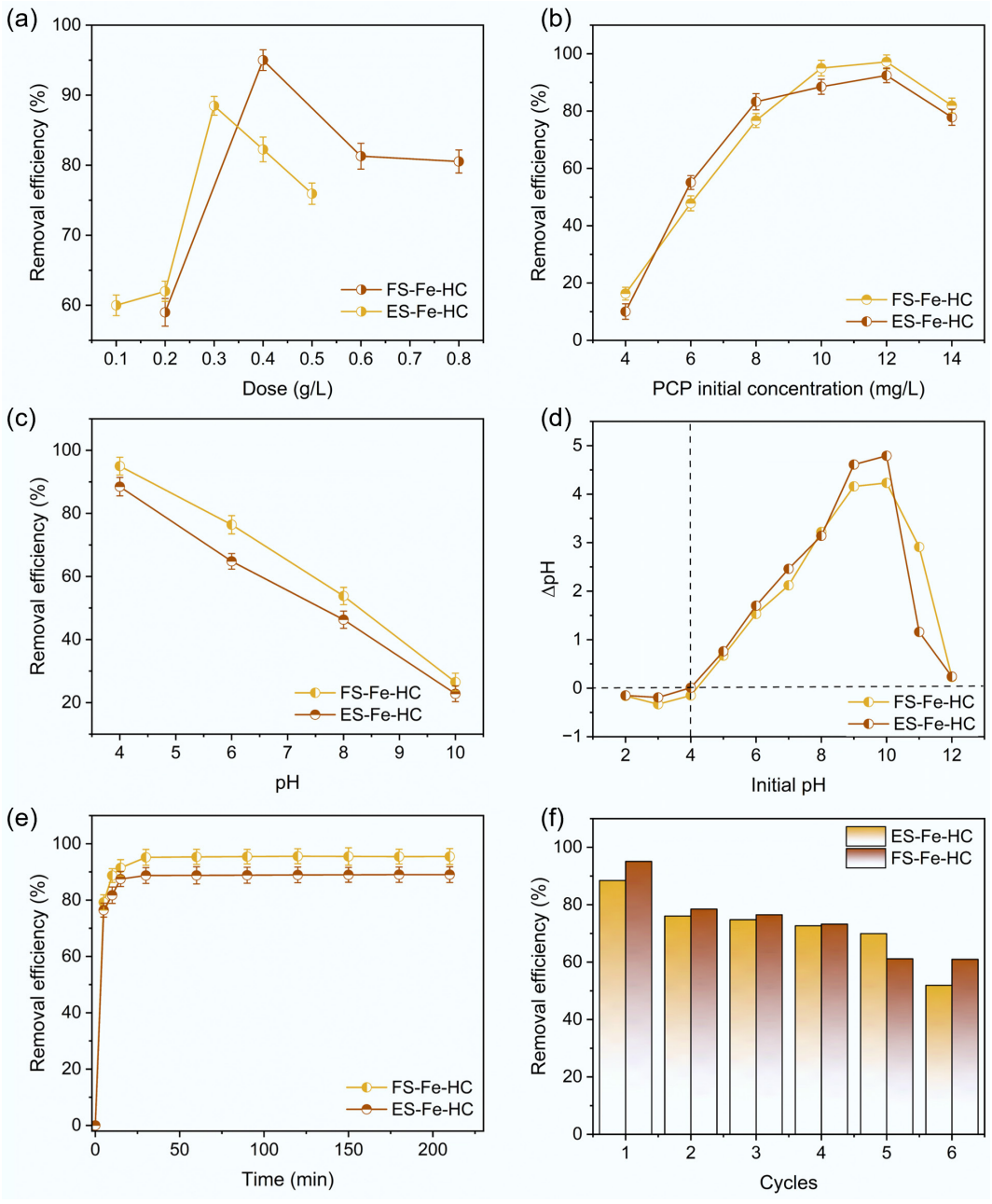

Fig. 6 Removal efficiency influenced by (**a**) adsorbent dose, (**b**) initial concentration of PCP, (**c**) pH, (**d**) point of zero charge, (**e**) contact time, and (**f**) reusability.

Table 3 Summary of different biomass waste-based adsorbents for PCP removal

Adsorbent	Adsorbent dose (g/L)	Time (h)	PCP (mg/L)	pH	Removal efficiency (%)	Ref.
Flax shives hydrochar	0.1	0.33	10	3	81	[25]
Fe_3O_4–SiO_2 decorated carbon nanotubes	0.5	2	100	2.5	98	[54]
Carbon nanotubes	0.35	1	1	–	88	[59]
Fungal biomass	1	6	1	3	100	[53]
Sunflower seed waste	40	1	5	2.5	84	[60]
FS-Fe-HC	0.4	1	10	4	95	This study
ES-Fe-HC	0.3	0.58	10	4	88	This study

Kinetics and isotherm analysis

Non-linear kinetic models were applied to evaluate the effect of reaction time on PCP adsorption by FS-Fe-HC and ES-Fe-HC. Unlike linearized forms, non-linear kinetic equations do not require prior assumptions about the experimental equilibrium adsorption capacity, which makes them more accurate and reliable for data fitting. Therefore, the non-linear approach is more appropriate and preferred for determining adsorption parameters[56]. Table 4 presents the parameters obtained by fitting non-linear kinetic models to PCP adsorption data. For adsorption using both FS-Fe-HC and ES-Fe-HC,

Table 4 Kinetics and isotherm models for PCP adsorption using FS-Fe-HC and ES-Fe-HC

			FS-Fe-HC	ES-Fe-HC
Kinetics	Pseudo-first order model	$Q_{e(exp)}$ (mg/g)	1.227	1.336
		$Q_{e(cal)}$ (mg/g)	1.21 ± 0.01	1.31 ± 0.008
		k_1 (min^{-1})	0.32 ± 0.02	0.001 ± 0.01
		R^2	0.995	0.997
		χ^2	0.0006	0.0005
	Pseudo-second order model	$Q_{e(cal)}$ (mg/g)	1.23 ± 0.01	1.36 ± 0.03
		k_2 (g/mg/min)	0.73 ± 0.14	1.0 ± 0.55
		R^2	0.992	0.969
		χ^2	0.001	0.005
Isotherm models	Langmuir model	Q_m (mg/g)	2.58 ± 0.64	57.99 ± 6.71
		K_L (L/mg)	0.63 ± 0.29	1.22 ± 0.34
		R_L	0.137	0.075
		R^2	0.928	0.957
		K_F	0.93 ± 0.09	28.92 ± 2.5
		χ^2	0.02	9.56
	Freundlich model	1/n	0.628	0.492
		n	1.59 ± 0.36	2.03 ± 0.44
		R^2	0.861	0.860
		χ^2	0.039	31.08
	Temkin model	A_T (L/g)	5.88 ± 0.76	10.51 ± 1.63
		b_T	0.583 ± 0.04	13.49 ± 0.98
		R^2	0.971	0.973
		χ^2	0.008	5.96

the pseudo-first order kinetic model showed better fitting when compared to the pseudo-second order model (Fig. 7a, b). A higher coefficient of correlation and the lowest χ^2 were observed, indicating good agreement in $Q_{e(cal)}$ and $Q_{e(exp)}$. Thus, it can be concluded that PCP adsorption was influenced by the available surface area of the hydrochar, allowing PCP molecules to form a surface layer and penetrate the adsorbent's pores[57]. To understand PCP adsorption on FS-Fe-HC and ES-Fe-HC, the Langmuir, Freundlich, and Temkin models were explored, with the non-linear fitting outcomes shown in Table 4 and Fig. 7c, d for comparing the better fitness of each model. Favorable adsorption was indicated by the R_L values, which fall in the range of 0 to 1. Among the models, the Temkin model provided the best fit for both hydrochars, indicating heterogeneous surfaces where the heat of adsorption decreases linearly with increasing surface coverage. The intensity-related coefficient (n) reflects the affinity of the adsorption process, where a value of $n > 1$ suggests the likelihood of physisorption[58]. The pH dependency of PCP adsorption also indicated the potential involvement of electrostatic attraction forces.

Recyclability of FS-Fe-HC and ES-Fe-HC post PCP adsorption

Reusing hydrochar-based adsorbents will lower operational costs and mitigate the environmental impact of the treatment process by increasing the longevity and reducing the need for additional resources[61]. The reusability potential of FS-Fe-HC and ES-Fe-HC was investigated through six treatment cycles of PCP contaminated water. It was observed that the adsorption capacity of the hydrochar

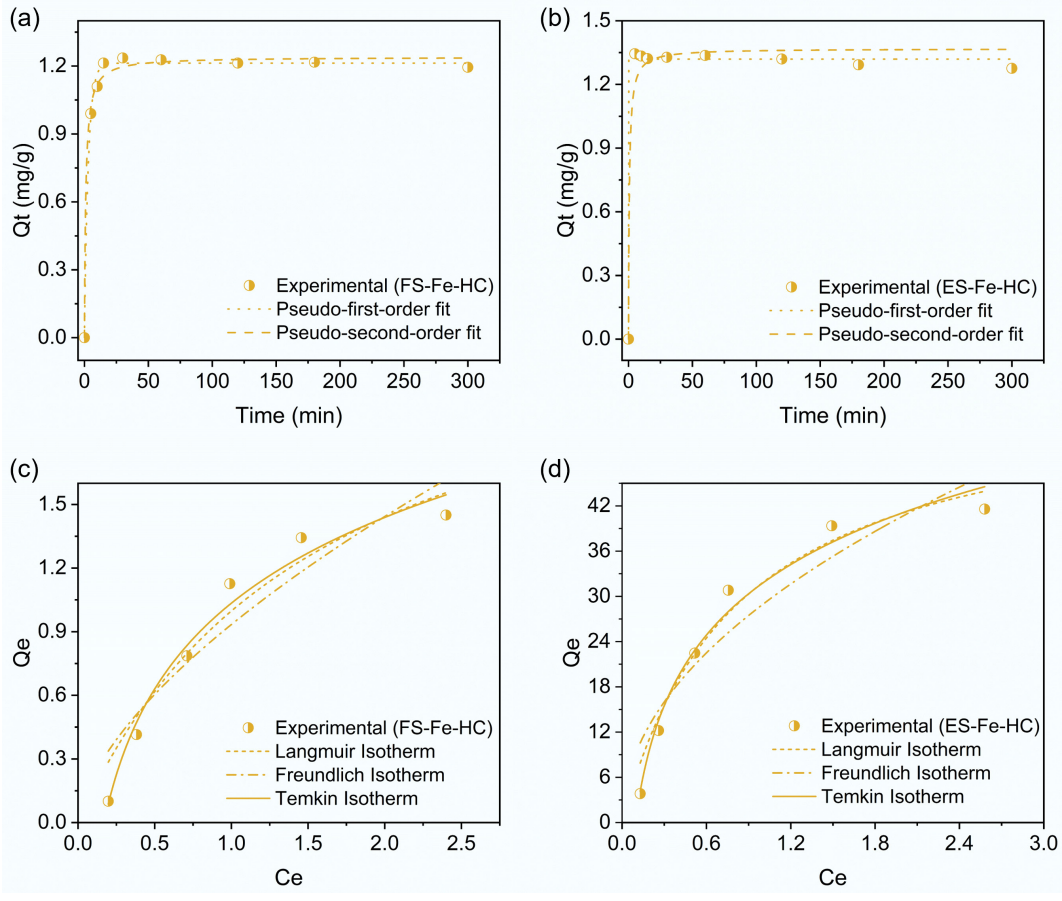

Fig. 7 Kinetic analysis of PCP adsorption using (**a**) FS-Fe-HC, and (**b**) ES-Fe-HC, and isotherm model fitting for PCP adsorption using (**c**) FS-Fe-HC, and (**d**) ES-Fe-HC.

gradually decreased by the end of the 6th cycle. The removal efficiency dropped from 95% to 60.98% for FS-Fe-HC and from 88% to 51.92% for ES-Fe-HC from cycle 1 to cycle 6, as shown in Fig. 6f. The results indicate that FS-Fe-HC was more efficient than ES-Fe-HC in the adsorption and desorption of PCP.

Leaching study

When applying magnetic adsorbents for wastewater treatment, it is crucial to evaluate the potential of iron leaching, as this could lead to secondary water pollution. To investigate the iron leaching behavior of the synthesized hydrochar, ICP spectroscopy was conducted. The results showed that there was no leaching of iron from either FS-Fe-HC or ES-Fe-HC throughout the entire PCP treatment process. Ensuring minimal to no iron leaching is vital for environmental safety as leached iron can introduce contaminants into the ecosystems, posing risks to water quality and aquatic life[62]. Moreover, iron leaching can diminish the magnetic properties of hydrochar, reducing its recyclability and efficiency in water remediation[63].

Conclusions

Magnetic hydrochar was successfully synthesized from flax shives and eucalyptus sawdust via HTC for the application in wastewater remediation. Under optimized conditions, FS-Fe-HC and ES-Fe-HC achieved PCP removal efficiencies of up to 95% and 88.5%, respectively. Comprehensive characterization through FTIR, XRD, XPS, SEM-EDS, and BET confirmed the presence of iron oxides, abundant surface functional groups, and well-developed mesoporous structures. The incorporation of iron not only provided magnetic properties, facilitating easy separation, but also significantly enhanced the specific surface area and porosity of the hydrochar, both of which are essential for efficient adsorption. The materials demonstrated strong reusability over multiple cycles with negligible performance loss and no detectable iron leaching, supporting their environmental safety and operational robustness.

This study presents a sustainable approach to valorizing agricultural and forestry biomass into functional adsorbents for removing the persistent contaminant pentachlorophenol. By aligning with circular economy principles and addressing key environmental challenges, these magnetic hydrochars show strong potential for scalable, low-cost wastewater treatment solutions.

Author contributions

All authors were involved in developing the study's concept and design. Tunnisha Dasgupta, Himadri Rajput, and Pubudi Perera were responsible for material preparation, data collection, and analysis. The first draft of the manuscript was written by Tunnisha Dasgupta and Himadri Rajput. Xiaohong Sun and Quan (Sophia) He provided feedback on the previous versions of the manuscript. All authors reviewed the results and approved the final version of the manuscript.

Data availability

The datasets used or analyzed during the current study are available from the corresponding author upon reasonable request.

Funding

The authors gratefully acknowledge funding from the Mitacs Globalink Research Internship program (ID: 129423), a Mitacs Elevate post-doctoral fellowship in partnership with Stella-Jones Inc. (NS-ISED IT34874), and funding from SSHRC-funded Sustainable Agriculture Research Initiative (1013-2024-0001).

Declarations

Competing interests

The authors declare that they have no conflict of interest.

Author details

[1]Department of Engineering, Faculty of Agriculture, Dalhousie University, Truro, NS B2N 5E3, Canada; [2]Department of Plant, Food and Environmental Sciences, Faculty of Agriculture, Dalhousie University, Truro, NS B2N 5E3, Canada

References

[1] LeRoy P. 1995. Troubled waters: population and water scarcity. *Colorado Journal of International Environmental Law and Policy* 6:299
[2] H_2O. 2022. How does industrial waste get into water systems and what are its effects. www.h2o-de.com/en/blog/how-does-industrial-waste-get-into-water-systems-and-what-are-its-effects
[3] U.S. Environmental Protection Agency. 1980. Ambient water quality criteria for pentachlorophenol. www.epa.gov/sites/default/files/2019-03/documents/ambient-wqc-pentachlorophenol-1980.pdf
[4] Bhattacharya SK, Yuan Q, Jin P. 1996. Removal of pentachlorophenol from wastewater by combined anaerobic-aerobic treatment. *Journal of Hazardous Materials* 49(2–3):143–154
[5] Patel UD, Suresh S. 2008. Electrochemical treatment of pentachlorophenol in water and pulp bleaching effluent. *Separation and Purification Technology* 61(2):115–122
[6] Ammeri RW, Hassen W, Hidri Y, Di Rauso Simeone G, Hassen A. 2022. Macrophyte and indigenous bacterial co-remediation process for pentachlorophenol removal from wastewater. *International Journal of Phytoremediation* 24(3):271–282
[7] Yang B, Xu D, Wu X, Li Z, Lei L, et al. 2015. Efficient removal of pentachlorophenol from wastewater by novel hydrophobically modified thermo-sensitive hydrogels. *Journal of Industrial and Engineering Chemistry* 25:67–72
[8] Li H, Lin M, Xiao T, Long J, Liu F, et al. 2020. Highly efficient removal of thallium(I) from wastewater via hypochlorite catalytic oxidation coupled with adsorption by hydrochar coated nickel ferrite composite. *Journal of Hazardous Materials* 388:122016
[9] Chai WS, Cheun JY, Kumar PS, Mubashir M, Majeed Z, et al. 2021. A review on conventional and novel materials towards heavy metal adsorption in wastewater treatment application. *Journal of Cleaner Production* 296:126589
[10] Ahmed S, Aktar S, Zaman S, Jahan RA, Bari ML. 2020. Use of natural biosorbent in removing dye, heavy metal and antibiotic-resistant bacteria from industrial wastewater. *Applied Water Science* 10:107
[11] Mohan D, Sarswat A, Ok YS, Pittman CU. 2014. Organic and inorganic contaminants removal from water with biochar, a renewable, low cost and sustainable adsorbent – a critical review. *Bioresource Technology* 160:191–202
[12] Davidson J. 1995. Ecological aspects of eucalyptus plantations. *Proceedings of the Regional Expert Consultation on Eucalyptus, 4–8 October 1993, Bangkok, Thailand*. FAO Regional Office for Asia and the Pacific. https://www.fao.org/4/ac777e/ac777e06.htm#fn4
[13] Perera P, Changotra R, Forren J, Green J, Hu Y, et al. 2025. Comprehensive review on flax shives – physicochemical properties and application potential. *Industrial Crops and Products* 225:120585
[14] Singh R, Dutta RK, Naik DV, Ray A, Kanaujia PK. 2021. High surface area *Eucalyptus* wood biochar for the removal of phenol from petroleum refinery wastewater. *Environmental Challenges* 5:100353
[15] Alqadami AA, Naushad M, ALOthman ZA, Alsuhybani M, Algamdi M. 2020. Excellent adsorptive performance of a new nanocomposite for removal of toxic Pb(II) from aqueous environment: adsorption

mechanism and modeling analysis. *Journal of Hazardous Materials* 389:121896

[16] Kang K, Hu Y, Khan I, He S, Fatehi P. 2023. Recent advances in the synthesis and application of magnetic biochar for wastewater treatment. *Bioresource Technology* 390:129786

[17] Aghababaei A, Borugadda VB, Dalai A, Niu CH. 2023. An investigation on adsorption of carbamazepine with adsorbents developed from flax shives: kinetics, mechanisms, and desorption. *Chemical Engineering Research and Design* 189:138–155

[18] Vievard J, Alem A, Pantet A, Ahfir ND, Devouge-Boyer C, et al. 2024. Non-competitive adsorption of polycyclic aromatic hydrocarbons and heavy metals on activated carbon produced from flax shives. *Emergent Materials* 8:2441–2450

[19] ASTM. 2021. Standard test method for ash in wood. *ASTM D1102-84(2021)*. ASTM, West Conshohocken, PA, USA. doi: 10.1520/D1102-84R21

[20] ASTM. 2019. Standard test method for volatile matter in the analysis of particulate wood fuels. *ASTM E872-82(2019)*. ASTM, West Conshohocken, PA, USA. doi: 10.1520/E0872-82R19

[21] ASTM. 2025. Standard test methods for direct moisture content measurement of wood and wood-based materials. *ASTM D4442-20*. ASTM, West Conshohocken, PA, USA. doi: 10.1520/D4442-20

[22] Lilian MJ, Bissessur R, Kang K, He QS, Hu Y. 2025. Study of KOH-activated hydrochar for CO_2 adsorption. *Journal of Industrial and Engineering Chemistry* 143:240–251

[23] Wang H, Liu Y, Ifthikar J, Shi L, Khan A, et al. 2018. Towards a better understanding on mercury adsorption by magnetic bio-adsorbents with γ-Fe_2O_3 from pinewood sawdust derived hydrochar: influence of atmosphere in heat treatment. *Bioresource Technology* 256:269–276

[24] Rajput H, Lan Q, Changotra R, Rajput P, Devi P, et al. 2025. Turning waste into value: Iron-cobalt bimetallic hydrochar for efficient removal of persistent chlorinated pollutants – mechanistic insights and adsorption models. *Catalysis Today* 454:115293

[25] Rajput H, Anh KN, Changotra R, Sun X, Zhong X, et al. 2025. Sustainable removal of organic pollutants using flax shives-derived hydrochar. *Biomass and Bioenergy* 202:108209

[26] Lang J, Matějová L, Cuentas-Gallegos AK, Lobato-Peralta DR, Ainassaari K, et al. 2021. Evaluation and selection of biochars and hydrochars derived from agricultural wastes for the use as adsorbent and energy storage materials. *Journal of Environmental Chemical Engineering* 9(5):105979

[27] Tan G, Sun W, Xu Y, Wang H, Xu N. 2016. Sorption of mercury (II) and atrazine by biochar, modified biochars and biochar based activated carbon in aqueous solution. *Bioresource Technology* 211:727–735

[28] Çatlıoğlu FN, Akay S, Gözmen B, Turunc E, Anastopoulos I, et al. 2020. Fe-modified hydrochar from orange peel as adsorbent of food colorant Brilliant Black: process optimization and kinetic studies. *International Journal of Environmental Science and Technology* 17(4):1975–1990

[29] Lam SS, Liew RK, Lim XY, Ani FN, Jusoh A. 2016. Fruit waste as feedstock for recovery by pyrolysis technique. *International Biodeterioration & Biodegradation* 113:325–333

[30] Hossain MD, Zhang Q, Cheng T, Goddard WA, Luo Z. 2021. Graphitization of low-density amorphous carbon for electrocatalysis electrodes from ReaxFF reactive dynamics. *Carbon* 183:940–47

[31] Luo X, Lei X, Cai N, Xie X, Xue Y, et al. 2016. Removal of heavy metal ions from water by magnetic cellulose-based beads with embedded chemically modified magnetite nanoparticles and activated carbon. *ACS Sustainable Chemistry & Engineering* 4(7):3960–3969

[32] Satira A, Paone E, Bressi V, Iannazzo D, Marra F, et al. 2021. Hydrothermal carbonization as sustainable process for the complete upgrading of orange peel waste into value-added chemicals and bio-carbon materials. *Applied Sciences* 11(22):10983

[33] Kundu S, Wang Y, Xia W, Muhler M. 2008. Thermal stability and reducibility of oxygen-containing functional groups on multiwalled carbon nanotube surfaces: a quantitative high-resolution XPS and TPD/TPR study. *The Journal of Physical Chemistry C* 112(43): 16869–16878

[34] Frankcombe TJ, Liu Y. 2023. Interpretation of oxygen 1s X-ray photoelectron spectroscopy of ZnO. *Chemistry of Materials* 35(14):5468–5474

[35] Kundu S, Nagaiah TC, Xia W, Wang Y, Dommele SV, et al. 2009. Electrocatalytic activity and stability of nitrogen-containing carbon nanotubes in the oxygen reduction reaction. *The Journal of Physical Chemistry C* 113(32):14302–14310

[36] Zhang X, Liu S, Wang M, Ma X, Sun X, et al. 2022. Hydrochar magnetic adsorbent derived from Chinese medicine industry waste *via* one-step hydrothermal route: Mechanism analyses of magnetism and adsorption. *Fuel* 326:125110

[37] Yi Y, Huang Z, Lu B, Xian J, Tsang EP, et al. 2020. Magnetic biochar for environmental remediation: a review. *Bioresource Technology* 298:122468

[38] Liu R, Zhang Y, Hu B, Wang H. 2022. Improved Pb(II) removal in aqueous solution by sulfide@biochar and polysaccharose-FeS@ biochar composites: efficiencies and mechanisms. *Chemosphere* 287:132087

[39] Davies G, McGregor J. 2021. Hydrothermal synthesis of biomass-derived magnetic carbon composites for adsorption and catalysis. *ACS Omega* 6(48):33000–33009

[40] Guo S, Gao Y, Wang Y, Liu Z, Wei X, et al. 2019. Urea/$ZnCl_2$ *in situ* hydrothermal carbonization of *Camellia sinensis* waste to prepare N-doped biochar for heavy metal removal. *Environmental Science and Pollution Research International* 26(29):30365–30373

[41] Pal N. 2020. Nanoporous metal oxide composite materials: a journey from the past, present to future. *Advances in Colloid and Interface Science* 280:102156

[42] Li Y, Hagos FM, Chen R, Qian H, Mo C, et al. 2021. Rice husk hydrochars from metal chloride-assisted hydrothermal carbonization as biosorbents of organics from aqueous solution. *Bioresources and Bioprocessing* 8:99

[43] Wang F, Guo C, Liu X, Sun H, Zhang C, et al. 2022. Revealing carbon-iron interaction characteristics in sludge-derived hydrochars under different hydrothermal conditions. *Chemosphere* 300:134572

[44] Xu Z, Zhou Y, Sun Z, Zhang D, Huang Y, et al. 2020. Understanding reactions and pore-forming mechanisms between waste cotton woven and $FeCl_3$ during the synthesis of magnetic activated carbon. *Chemosphere* 241:125120

[45] Mane PV, Rego RM, Yap PL, Losic D, Kurkuri MD. 2024. Unveiling cutting-edge advances in high surface area porous materials for the efficient removal of toxic metal ions from water. *Progress in Materials Science* 146:101314

[46] Chen D, Cen K, Zhuang X, Gan Z, Zhou J, et al. 2022. Insight into biomass pyrolysis mechanism based on cellulose, hemicellulose, and lignin: evolution of volatiles and kinetics, elucidation of reaction pathways, and characterization of gas, biochar and bio-oil. *Combustion and Flame* 242:112142

[47] Wang F, Liu X, Guo C, Lian F, Li Z, et al. 2024. A novel cobalt-iron bimetallic hydrochar for the degradation of triclosan in the aqueous solution: performance, reusability, and synergistic degradation mechanism. *Environmental Pollution* 358:124487

[48] Mondal P, Majumder CB, Mohanty B. 2008. Effects of adsorbent dose, its particle size and initial arsenic concentration on the removal of arsenic, iron and manganese from simulated ground water by Fe^{3+} impregnated activated carbon. *Journal of Hazardous Materials* 150(3):695–702

[49] Sun Y, Wang T, Han C, Bai L, Sun X. 2023. One-step preparation of lignin-based magnetic biochar as bifunctional material for the efficient removal of Cr(VI) and Congo red: Performance and practical application. *Bioresource Technology* 369:128373

[50] Zenasni MA, Benfarhi S, Merlin A, Molina S, George B, et al. 2012. Adsorption of Cu(II) on maghnite from aqueous solution: effects of pH, initial concentration, interaction time and temperature. *Natural Science* 4(11):856–868

[51] Chien SC, Chen SH, Li CJ. 2018. Effect of soil pH and organic matter on the adsorption and desorption of pentachlorophenol. *Environmental Science and Pollution Research* 25(6):5269–5279

[52] Peng P, Lang YH, Wang XM. 2016. Adsorption behavior and mechanism of pentachlorophenol on reed biochars: pH effect, pyrolysis

temperature, hydrochloric acid treatment and isotherms. *Ecological Engineering* 90:225–233

[53] Mathialagan T, Viraraghavan T. 2009. Biosorption of pentachlorophenol from aqueous solutions by a fungal biomass. *Bioresource Technology* 100(2):549–558

[54] Zhou L, Pan S, Chen X, Zhao Y, Zou B, et al. 2014. Kinetics and thermodynamics studies of pentachlorophenol adsorption on covalently functionalized Fe_3O_4@SiO_2–MWCNTs core–shell magnetic microspheres. *Chemical Engineering Journal* 257:10–19

[55] Rasouli Sadabad H, Coleman HM, Dooley JSG, Snelling WJ, O'Hagan B, et al. 2024. Desorption of antibiotics from granular activated carbon during water treatment by adsorption. *Environmental Processes* 11(4):64

[56] Widiartyasari Prihatdini R, Suratman A, Siswanta D. 2023. Linear and nonlinear modeling of kinetics and isotherm of malachite green dye adsorption to trimellitic-modified pineapple peel. *Materials Today: Proceedings* 88:33–40

[57] Rao MA, Di Rauso Simeone G, Scelza R, Conte P. 2017. Biochar based remediation of water and soil contaminated by phenanthrene and pentachlorophenol. *Chemosphere* 186:193–201

[58] Anwar Mohamad Said K, Zakirah Ismail N, Liyana Jama'in R, Ain Mohamed Alipah N, Mohamed Sutan N, et al. 2018. Application of freundlich and temkin isotherm to study the removal of Pb(II) via adsorption on activated carbon equipped polysulfone membrane. *International Journal of Engineering & Technology* 7:91

[59] Abdel Salam M, Burk RC. 2010. Thermodynamics and kinetics studies of pentachlorophenol adsorption from aqueous solutions by multi-walled carbon nanotubes. *Water, Air, & Soil Pollution* 210:101–111

[60] Kuśmierek K, Dąbek L, Świątkowski A. 2018. Adsorptive removal of pentachlorophenol from water using agricultural and industrial wastes. *Desalination and Water Treatment* 117:142–148

[61] El Messaoudi N, El Khomri M, El Mouden A, Bouich A, Jada A, et al. 2024. Regeneration and reusability of non-conventional low-cost adsorbents to remove dyes from wastewaters in multiple consecutive adsorption–desorption cycles: a review. *Biomass Conversion and Biorefinery* 14(11):11739–11756

[62] Bakker ES, Van Donk E, Immers AK. 2016. Lake restoration by in-lake iron addition: a synopsis of iron impact on aquatic organisms and shallow lake ecosystems. *Aquatic Ecology* 50:121–135

[63] Meng H, Chen Z, Wei W, Xu J, Duan H, et al. 2025. Magnetic hydrochar for sustainable wastewater management. *NPJ Materials Sustainability* 3:7